Separation Science and Technology
Publication details, including instructions for authors and subscription information:
http://www.informaworld.com/smpp/title~content=t713708471

A Novel Adsorption Cycle for CO_2 Recovery: Experimental and Theoretical Investigations of a Temperature Swing Compression Process

Krista S. Walton[a]; M. Douglas LeVan[a]
[a] Department of Chemical Engineering, Vanderbilt University, Nashville, TN, USA

To cite this Article Walton, Krista S. and LeVan, M. Douglas(2006) 'A Novel Adsorption Cycle for CO_2 Recovery: Experimental and Theoretical Investigations of a Temperature Swing Compression Process', Separation Science and Technology, 41: 3, 485 — 500
To link to this Article: DOI: 10.1080/01496390500524834
URL: http://dx.doi.org/10.1080/01496390500524834

Separation Science and Technology, 41: 485–500, 2006

ISSN 0149-6395 print/1520-5754 online
DOI: 10.1080/01496390500524834

A Novel Adsorption Cycle for CO_2 Recovery: Experimental and Theoretical Investigations of a Temperature Swing Compression Process

Krista S. Walton and M. Douglas LeVan
Department of Chemical Engineering, Vanderbilt University, Nashville, TN, USA

Abstract: A novel adsorption cycle is examined experimentally and theoretically for recovering carbon dioxide from a 50 mol% mixture with carbon monoxide. Several adsorbents are considered, and zeolite NaY is chosen for the process due to its high capacity and selectivity for CO_2 in the presence of CO. The process consists of three steps. The bed is fed the gas mixture at 273 K until CO_2 breakthrough occurs. The bed then undergoes countercurrent blowdown of CO_2 while heating at 391 K and is finally cooled to the initial feed temperature once the bed has been depleted of CO_2. Results are presented from laboratory scale experiments and are described using numerical simulations. This novel cycle provides a method for capturing and producing CO_2 without the need for a purge gas and has low energy requirements if waste heat is available.

Keywords: Fixed-bed adsorption, nonisothermal effects, CO_2 capture, pressure swing, temperature swing compression

INTRODUCTION

The need for separating mixtures of carbon dioxide and carbon monoxide arises in many industrial applications. Hydroformylation from synthesis gas

Received 16 March 2005, Accepted 27 November 2005
Address correspondence to M. Douglas LeVan, Department of Chemical Engineering, Vanderbilt University, VU Station B #351604, 2301 Vanderbilt Place, Nashville, TN 37235-1604, USA. Tel.: (615) 322-2441; Fax: (615) 343-7951; E-mail: m.douglas.levan@vanderbilt.edu

requires pure CO and hydrogen. Mixtures of CO and H_2 are also used for reducing oxides in ores to base metals and for the production of methanol. Carbon monoxide is considered to be a valuable gas for producing many different chemicals such as acetic acid, acrylic acid, and phosgene, and also has the potential to be used as a low-grade fuel as the natural gas supply is depleted (1, 2). Most sources of CO are gas mixtures containing CO_2, H_2, and N_2 (2). Hence, the separation of CO from these gases is important for a variety of applications.

In addition to separations of carbon dioxide and carbon monoxide, recovery of carbon dioxide is important in many processes. The combustion of fossil fuels results in large emissions of CO_2. As such, the separation and capture of CO_2 from flue gas has received much attention due to increasing concerns on global warming. It is also a frequent contaminant in natural gas, and due to the lower volatility of CO_2, it will interfere with the adsorptive storage of methane. CO_2 is often used in the food and beverage industry, pulp and paper applications, and water treatment processes.

Aside from the industrial relevance, the separation of CO_2 and CO is of particular interest for NASA's Mars in-situ resource utilization program (ISRU). This separation is part of a three-step process (3, 4) for producing oxygen from the atmosphere of Mars, which is 95% CO_2. The atmospheric pressure on Mars is approximately 0.007 bar and must be compressed to 1 bar to be used in the production of oxygen. Thus, the first step of this process uses an adsorption compressor that takes in the Mars atmosphere at low pressure and delivers CO_2 at a pressure of 1 bar. This provides the feed stream for the second process component, which is a solid oxide electrolysis cell. This step produces O_2 and CO from CO_2. There will be unreacted CO_2 that will exit the cell in an approximately 50 mol% mixture with CO. The separation of this mixture allows the CO_2 to be fed back into the process, which will favorably impact the adsorption compressor requirement in the first step because it will cut down on the amount of atmospheric CO_2 that must be compressed.

Adsorption-based separation processes operate by taking advantage of differences in adsorption equilibrium, diffusion rates of the different molecules, or size exclusion of components due to adsorbent pore sizes. The best adsorbent for the application is determined by its capacity or by differences in intraparticle diffusivities in the desired operating temperature and pressure range. In addition to pure- and multi-component adsorption isotherms, the desired product purities, method of regeneration, and required loading swings must all be considered when designing the separation process (5, 6).

Pressure swing adsorption (PSA) processes have been studied extensively for removing CO_2 from exhaust gases (7–16) and offer advantages such as low energy requirements and cost savings compared to other methods such as absorption or membrane separation and typically operate by equilibrium separation. Many PSA separations operate with short cycle times, which gives high-throughput systems; this is especially important when treating

bulk amounts of CO_2 in exhaust streams (9). However, a typical PSA separation results in an impure waste stream at low pressure; this is a complication if the goal is to recover and use the more strongly adsorbed component. A temperature swing adsorption process would also create a waste stream, which again is not desirable for certain process requirements.

For our NASA application here, CO_2 recovery is much different from removing CO_2 from exhaust gases. The cycles described above all require the use of a mechanical compressor or vacuum pump. This would not be feasible for an application in Mars ISRU because of maintenance issues. The cycle must be as simple as possible to be successful in the harsh environment of Mars. A temperature swing compression process (3, 4) can provide an excellent solution to this problem.

Our objective in this work is to develop a CO/CO_2 separation process in which CO_2 is selectively removed from a 50 mol% mixture with CO, resulting in CO production during the feed step and CO_2 production during blowdown. We investigate a novel temperature swing compression cycle to achieve this separation. We discuss selection of the proper adsorbent based on adsorption equilibrium measurements, describe the process cycle, and present experimental and mathematical modeling results for the separation process.

ADSORBENT SELECTION

Selection of the proper adsorbent is the most crucial step when designing a new adsorption process. For CO_2 recovery in the process considered here, a material is needed that will selectively adsorb CO_2 in the presence of CO. Because the process requires that we also produce CO_2 during the blowdown step, we need a material for which CO_2 isotherms have the proper shape, i.e., fairly linear as opposed to rectangular. The gravimetric method was used to screen adsorbents for CO_2-selective adsorption. This method provides a means for quickly determining which adsorbents warrant further study over a wider range of conditions. Pure-component adsorption equilibrium data for CO_2 on BPL carbon, silicalite, and zeolites 3A, 4A, 5A, NaX, and NaY were measured at 25°C. All zeolites were 1/16 inch pellets obtained from UOP. As shown in Fig. 1, NaY, NaX, and 5A have the highest capacities for CO_2.

Pure-component adsorption equilibrium data for CO were also measured on these adsorbents using the gravimetric method. From Fig. 2, the isotherms indicate that CO will not compete very well with CO_2 for adsorption on NaX or NaY zeolite. It was also found that the CO_2 isotherm for NaY is more linear in the low pressure region than the isotherm for NaX. Based on these results, NaY was chosen as the best adsorbent for selectively adsorbing CO_2 from a mixture with CO.

Because our process will operate at high temperatures, adsorption isotherms for CO_2 on NaY were measured at 25°C, 75°C, and 125°C, and for CO at 25°C, 50°C, and 75°C using the volumetric method. These are

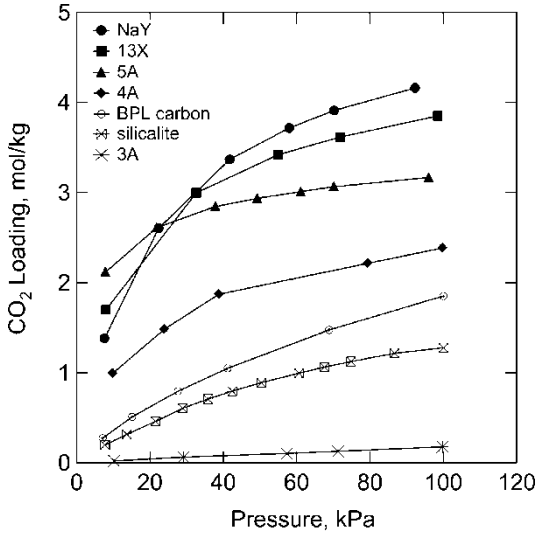

Figure 1. Adsorption isotherms of CO_2 on various adsorbents at 25°C.

shown in Fig. 3. Isotherms could not be measured for CO above 75°C because the adsorbed amount was too small to be detected by our experimental system. It is clear from Fig. 3 that NaY has a much greater affinity and capacity for CO_2 than for CO. Measured loadings for CO_2 are at least one order of magnitude greater than CO loadings.

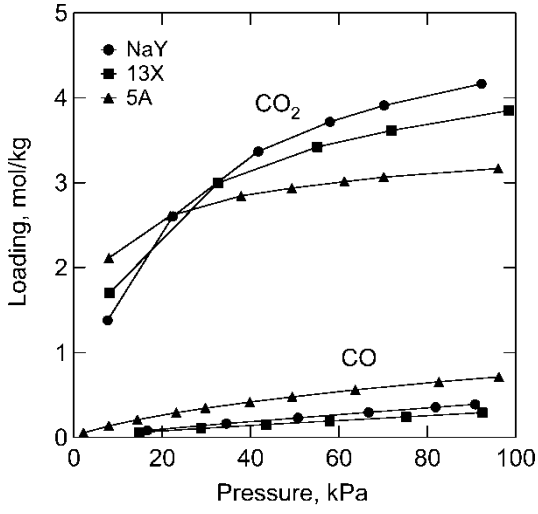

Figure 2. Pure-component adsorption isotherms of CO_2 and CO on zeolites NaY, 13X, and 5A at 25°C.

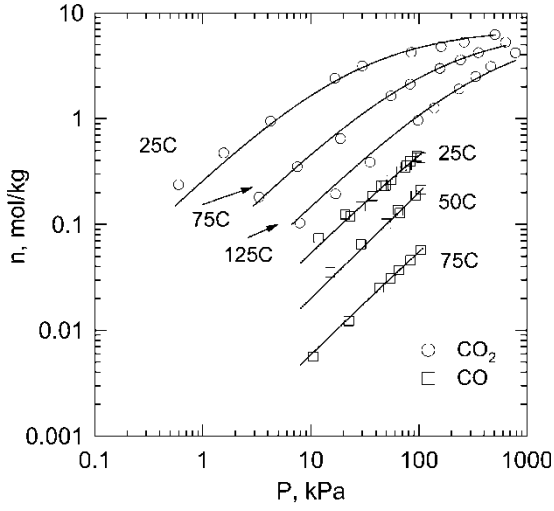

Figure 3. Pure-component adsorption isotherms of CO_2 and CO on zeolite NaY at various temperatures. Curves were calculated using the Toth equation.

While pure-component data indicate that NaY is a good choice for the separation process, the cycle must work to recover CO_2 from a 50 mol% mixture with CO. Thus, it is necessary to understand competitive adsorption effects of the two adsorbates. Binary adsorption equilibrium data were measured volumetrically for CO/CO_2 mixtures on NaY zeolite at 298 K. The closed-loop system with a fixed bed of adsorbent was initially charged with CO_2 and then CO was added. Since CO_2 adsorbs strongly compared to CO, the initial loading remains essentially constant as the CO is added to the system. This method allows control over the experimental composition and also reaches equilibrium faster than occurs by injecting the mixture or injecting CO first.

Experimental results are shown in Fig. 4. This figure shows pure-component isotherms for CO and CO_2 at 298 K for comparison with the binary data. For the binary measurements, CO_2 was adsorbed at an equilibrium pressure of about 8 kPa. Carbon monoxide was then coadsorbed at a partial pressure of approximately 100 kPa. It can be seen in the figure that CO_2 adsorption (closed circles) is relatively unaffected by the presence of CO, but the CO loading (closed squares) is only half of its pure-component value. As the partial pressure of CO_2 in the system is increased, we find that CO begins to desorb. This is shown by the vertical decrease in loading of CO in Fig. 4. These results confirm that CO does not compete significantly with CO_2 for adsorption on NaY zeolite. This is the desired behavior for selectively separating CO_2 from mixtures with CO.

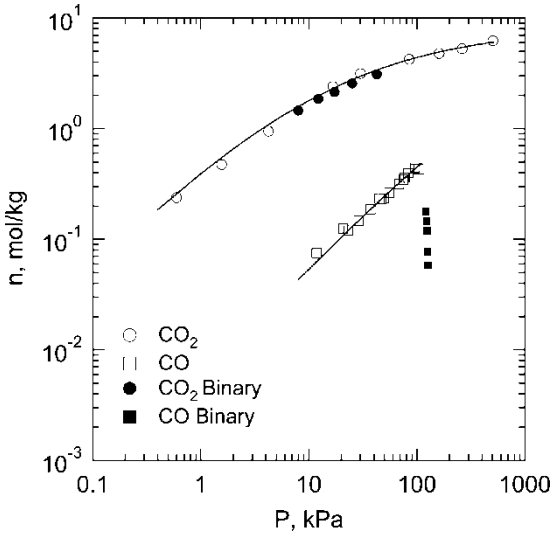

Figure 4. Adsorption equilibria of CO and CO_2 on NaY. Open symbols are pure-component measurements. Closed symbols are binary measurements. Note the drop in CO loading as CO_2 is added to the system.

RECOVERY AND COMPRESSION PROCESS

With the goal being to produce nearly pure CO during the feed step and nearly pure CO_2 during blowdown, we consider a novel three-step cycle that combines aspects of temperature swing adsorption and compression cycles such that no purge gas is required and no waste stream is created. This is particularly important for the NASA application. The purpose of the cycle then is to recover CO_2 from a 50% mixture with CO and compress it to a final pressure of 100 kPa. This final condition is required in order to recycle the CO_2 into the oxygen production process. As illustrated in Fig. 5, the first step consists of feeding a 50 mol% mixture of CO and CO_2 at a total pressure of 100 kPa into a fixed bed of NaY zeolite at 273 K. CO is produced until the bed is saturated with CO_2. Upon saturation, the bed undergoes countercurrent blowdown of CO_2 at 391 K and a pressure of 100 kPa. One of the goals is to deliver the CO_2 at a pressure of 1 bar, so blowdown continues until the gas discharge flow decreases to a low value. The bed is finally cooled to the feed temperature of 273 K with no gas flow, which completes the cycle.

Experiments

The separation device used in the process is shown in Fig. 6. It is constructed of stainless steel with two Viton O-rings placed in the top cap for sealing

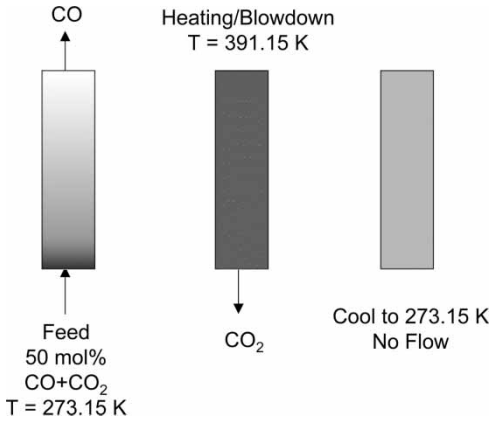

Figure 5. Illustration of three-step adsorption cycle.

purposes. The bed volume is approximately 100 cc and can accommodate 40 g of zeolite pellets. The device is heated or cooled in an environmental chamber, as shown in the illustration in Fig. 7, and mass flow controllers allow constant feed of the mixture at prescribed rates. Valving controls the direction of gas flow, i.e., switching from feed to countercurrent blowdown. A mass flow meter was placed on the product side to measure the flowrate during feed and blowdown, and a gas chromatograph (GC) was used to analyze the composition of the product stream. A pressure controller was used to maintain the total pressure of the bed at 1 atm during all process steps. The process was automated using National Instrument's LabView software.

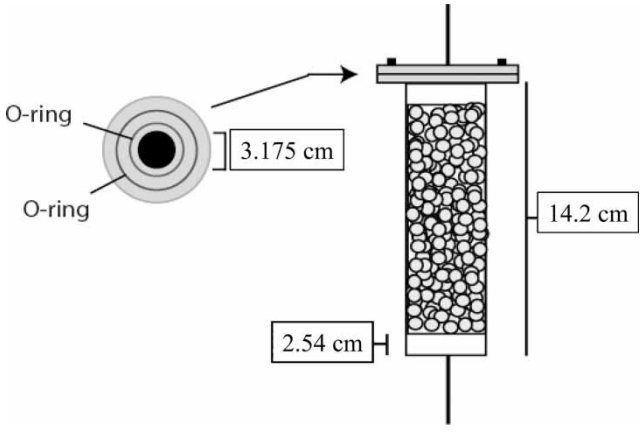

Figure 6. Schematic of separation device.

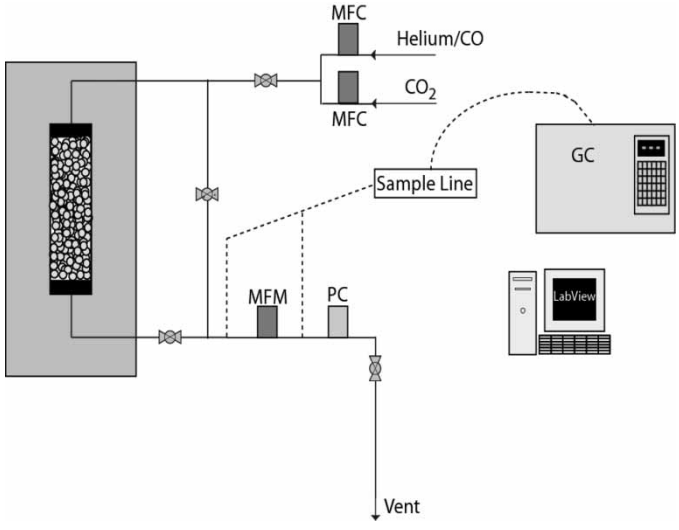

Figure 7. Experimental set-up for conducting CO/CO_2 adsorptive separation process.

Mathematical Model

Based on the results of our binary adsorption measurements, we assume that CO adsorption is negligible. Thus, CO_2 adsorption can be described by a pure-component isotherm model. The multi-temperature Toth equation was used in the simulations to describe adsorption equilibria of CO_2 on NaY zeolite. The isotherm is given by (17)

$$n = n_s \left(\frac{b + P_{CO2}^t}{P_{CO2}^t} \right)^{(-1/t)} \tag{1}$$

where CO_2 pressure is in kPa, n_s is the monolayer capacity and t and b are Toth parameters with b given by

$$b = b_0 \exp(-t\lambda/RT) \tag{2}$$

where λ is the isosteric heat of adsorption. The parameters are listed in Table 1.

The basis for our heat and mass transfer analysis of the cycle is found in the models of Farooq et al. (18) and Mahle et al. (19) The following assumptions are made for our process.

1. The ideal gas law applies.
2. Pressure drop across the bed is neglected.
3. Axial dispersion is neglected.

Table 1. Toth parameters for CO_2 adsorption

t	0.727
b_0	4.675×10^4
n_s	7.128 mol/kg
λ	28.74 kJ/mol

4. Mass transfer rate is described by the linear driving force (LDF) approximation.
5. Concentration, velocity, and temperature gradients in the radial direction are neglected, and radial heat transfer is treated using overall heat transfer coefficients.
6. Heat transfer can occur between column wall/surroundings, column wall/packed bed.
7. CO is treated as inert.
8. Heat capacities of both gases are assigned constant gas-phase values, which is consistent with the thermodynamic path used to develop the energy balance (20, 21).
9. The isosteric heat of adsorption is constant.
10. Heat and mass transfer coefficients are constant.
11. Physical properties of the adsorbent and column wall are constant.
12. Following PSA modeling (18, 19), gas molar concentration changes are dominated by pressure effects in comparison to thermal effects. Parameters used in the simulations are shown in Table 2.

Applying the above assumptions, the following equations are obtained and solved numerically (7).

Overall material balance:

$$\rho_b \frac{\partial n}{\partial t} + \frac{\varepsilon'}{RT_{step}} \frac{dP}{dt} + \frac{P}{RT_{step}} \frac{\partial v}{\partial z} = 0 \tag{3}$$

Component material balance:

$$\rho_b \frac{\partial n_i}{\partial t} + \frac{\varepsilon'}{RT_{step}} \left[P \frac{\partial y_i}{\partial t} + y_i \frac{\partial P}{\partial t} \right] + \frac{1}{RT_{step}} \left[y_i P \frac{\partial v_i}{\partial z} + v_i P \frac{\partial y_i}{\partial z} \right] = 0 \tag{4}$$

where T_{step} is 273 K for the feed step and 391 K for the blowdown step.

Energy balance for column wall:

$$m_w C_{pw} \frac{\partial T_w}{\partial t} = -U_1 (T_w - T) - U_2 (T_w - T_{env}) \tag{5}$$

where the bed temperature, T, and the wall temperature, T_w, vary with axial position, and the overall heat transfer coefficients are used to account for radial heat transfer.

Table 2. System parameters

C°_{pg} CO_2	33.58 J/(mol K)
C°_{pg} CO	29.18 J/(mol K)
C_{sol}	920.0 J/(kg K)
C_{pw}	460.0 J/(kg K)
ρ_b	397.08 kg/m^3
ε'	0.7
R_p	7.937×10^{-4} m
L_{bed}	0.122 m
d_{bed}	3.175 cm
m_w	0.165 kg
m_{sol}	0.040 kg

Energy balance for fluid phase:

$$\rho_b \frac{\partial u_s}{\partial t} + \varepsilon' \frac{\partial (c u_f)}{\partial t} + \frac{\partial (v c h_f)}{\partial z} = -U_1 (T - T_w) \tag{6}$$

where internal energies and the enthalpy of the fluid phase are represented by

$$u_s = (C_{sol} + C^{\circ}_{pg}\, n)(T - T_{ref}) - \lambda n \tag{7}$$

$$u_f = h_f - RT \tag{8}$$

$$h_f = C^{\circ}_{pg}\,(T - T_{ref}) \tag{9}$$

and

$$C^{\circ}_{pg}\, c = \sum_i C^{\circ}_{pgi}\, c_i \tag{10}$$

The mass transfer rate is described by the LDF equation

$$\frac{\partial n}{\partial t} = k_n (n^* - n) \tag{11}$$

where n^* is the equilibrium loading, and the mass transfer coefficient is given by (22)

$$k_n = \frac{15\, \psi D_s}{R_p^2} \tag{12}$$

where $\psi = 19/15$ and the diffusivity is determined from the correlation of Sladek et al. (23)

$$D_s(m^2/s) = 1.6 \times 10^{-6} \exp(-0.45\, q_{diff}/RT) \tag{13}$$

where

$$q_{diff} = \lambda - RT \tag{14}$$

All spatial derivatives can be written in backward difference form, resulting in a set of coupled first-order ordinary differential equations. The number of differences (volumes, mixing cells, or stages) is chosen such that there is no effect on the calculations, e.g., the results for 40 differences are the same as those for 80 differences.

Determination of Heat Transfer Coefficients

Heat transfer coefficients used in our mathematical model for describing the column wall and packed bed were determined by independent experiments. Measured values were preferred as opposed to obtaining values that correspond to the best fit of the separation process data. Thermocouples were placed in the center of the environmental chamber, against the outside wall of the separation device, and inside the bed. The temperature change with time was recorded for all three locations as the chamber was heated to the blowdown temperature of 391 K from the feed temperature of 273 K.

The air surrounding the separation device in the environmental chamber reached a maximum temperature of 391 K. The change in temperature with time was described by the following equation

$$T_{env} = T_{max} - (T_{max} - T_{init}) \exp(-0.0883t) \tag{15}$$

where T_{max} and T_{init} are 391 K and 273 K, respectively, and t has units of minutes. The measured temperature and the curve described by Eq. (15) are shown in Fig. 8.

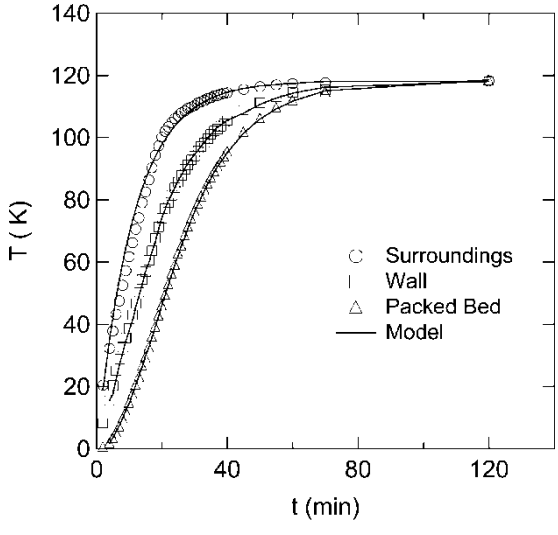

Figure 8. Temperature change with time and model calculations from eqs. (15–17).

The value for U_1, which is the heat transfer coefficient for the packed bed, was determined from the energy balance:

$$m_{sol}C_{sol}\frac{\partial T}{\partial t} = U_1(T_w - T) \tag{16}$$

where T is the temperature of the bed and T_w is the wall temperature. In a similar way, the heat transfer coefficient for the wall of the separation device, U_2, was determined using an energy balance for the wall given by

$$m_w C_w \frac{\partial T_w}{\partial t} = U_2(T_{env} - T_w) - U_1(T_w - T) \tag{17}$$

The values for U_1 and U_2 were found to be $7.33 \times 10^{-2}\,\mathrm{J/(s\,K)}$ and $0.217\,\mathrm{J/(s\,K)}$, respectively. The measured temperature data are shown in Fig. 8 plotted versus time. The figure shows that the calculated heat transfer coefficients lead to good predictions of temperature changes for all three locations.

RESULTS AND DISCUSSION

A feed mixture of 50 mol% CO_2 and CO at a total flowrate of 100 cc/min was used in the experiments. As seen in Fig. 9, CO_2 begins to breakthrough the bed about 1 hour and 10 minutes after the feed step has begun for the first cycle.

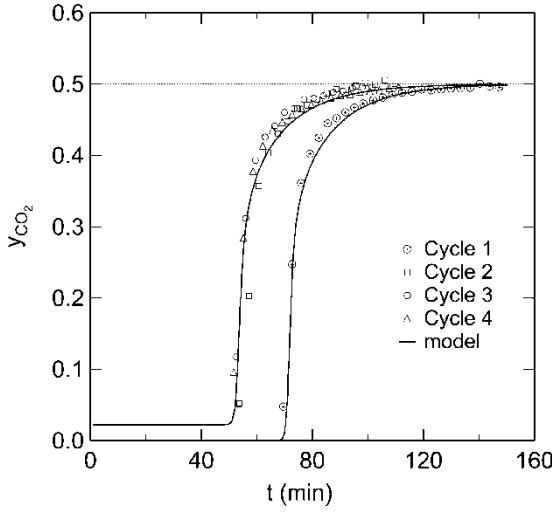

Figure 9. Breakthrough curves for CO_2 on NaY zeolite. Symbols are experimental data; curves are model predictions.

For subsequent cycles, CO_2 breakthrough occurs earlier after a feed duration of approximately 55 minutes. The first cycle takes longer to breakthrough because the cycle begins with a clean bed. So, cycles 2, 3, and 4 breakthrough faster than the first cycle because a small amount of CO_2 is left in the bed at the end of the first cycle. Before CO_2 breakthrough, approximately pure CO, within GC detection limits ($y_{CO_2} < 0.03$), is being produced during each cycle. The results of our mathematical model are also shown in Fig. 9. We obtained good agreement between simulations and experimental results. Simulations performed in which CO was allowed to coadsorb with CO_2 did not change the predicted breakthrough curve significantly. This result verifies our assumption that CO can be treated as inert gas.

Negligible amounts of CO are coadsorbed with CO_2 during the feed step, so relatively pure CO_2 is produced during blowdown. Figure 10 shows the flowrate of CO_2 out of the bed during heating and blowdown. Most of the CO_2 has exited the bed after one hour of heating, which coincides with the time needed to heat the bed to the blowdown temperature of 391 K. There is, in fact, approximately 1 mol/kg of CO_2 left in the bed at the conclusion of blowdown. At the end of the cooling step, this CO_2 loading corresponds to roughly 1 kPa of CO_2 in the system, which contributes to faster breakthrough times as discussed for Fig. 9. As shown in Fig. 10, the model provides a good qualitative prediction of the observed behavior. A more accurate fit of the experimental data could be achieved by adjusting some of the physical parameters in the model such as increasing the heat capacity of the wall, but we have chosen to determine parameters using independent measurements, as described in the previous section.

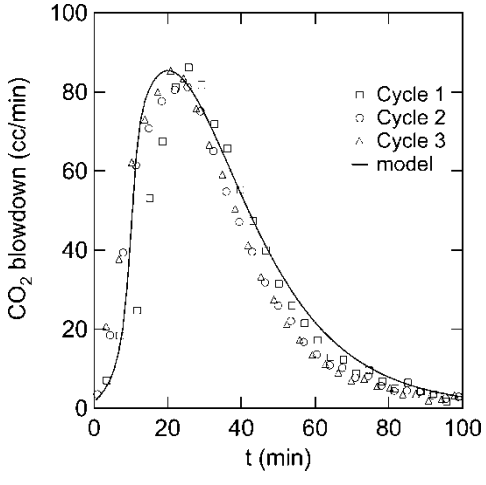

Figure 10. Flowrate of CO_2 exiting the separation device during heating and blowdown. Symbols are experimental data; curve is model prediction.

An important feature of this simple three-step cycle is that no purge gas is required to remove the more strongly adsorbed component. This circumvents the problem of handling an impure waste stream; CO is produced from the feed, and CO_2 is produced during blowdown. The blowdown step does require a large temperature swing, but this energy can be easily supplied by other components in the NASA process for generating oxygen from the Martian atmosphere. The mode of heating and cooling could depend on the size of the column. A small column like that used in the experiments could be uninsulated and heated and cooled externally. A large column could be heated and cooled using a heat transfer fluid flowing through tubes or slots passing through the bed.

CONCLUSIONS

A three-step adsorption cycle has been developed for the recovery of CO_2 from mixtures with CO. The process consists of a feed step at 273 K, heating and countercurrent blowdown at 391 K, and a final cooling step to complete the cycle. The process allows production of CO during the feed step and CO_2 during blowdown. Laboratory scale experiments using NaY zeolite as the adsorbent were performed, and the experiments were simulated using a mathematical model. The cycle runs without the use of a purge gas for the blowdown step. This type of cycle would be useful for separation processes in which waste heat is available for providing the temperature swing.

NOTATION

c	gas-phase concentration, mol/m^3
C_{pg}°	ideal gas heat capacity, J/(mol K)
C_{sol}	heat capacity of the solid, J/(kg K)
C_{pw}	heat capacity of the wall, J/(kg K)
h_f	fluid-phase enthalpy, J/mol
m_{sol}	mass of adsorbent, kg
m_w	mass of wall, kg
n	loading, mol/kg
P	pressure, Pa
R	ideal gas constant, J/(mol K)
T	temperature inside the bed, K
T_{env}	temperature of environmental chamber, K
T_w	wall temperature, K
U_1	heat transfer coefficient of packed bed, J/(s K)
U_2	heat transfer coefficient of separation device wall, J/(s K)
u_s	internal energy of stationary phase, J/(kg K)
v	superficial velocity, m/s

z	axial coordinate, m

Greek Letters

$\varepsilon' =$	total bed voidage
$\lambda =$	isosteric heat of adsorption, J/mol
$\rho_b =$	bulk density of packing, kg/m^3

ACKNOWLEDGEMENTS

We are grateful to the National Aeronautics and Space Administration and the Office of Biological and Physical Research for the support of this research under Fluid Physics Grant NAG3-2401.

REFERENCES

1. Xie, Y., Zhang, J., Qiu, J., Tong, X., Fu, J., Yang, G., Yan, H., and Tang, Y. (1996) Zeolites modified by CuCl for separating CO from gas mixtures containing CO_2. *Adsorption*, 3: 27–32.
2. Dutta, N.N. and Patil, G.S. (1995) Developments in CO separation. *Gas Separation & Purification*, 9 (4): 277–283.
3. LeVan, M.D., Walton, K.S., Finn, J.E., and Sridhar, K.R. (2002) Separation of carbon monoxide and carbon dioxide for Mars ISRU, Abstracts and presentations for plenary and sessions 1–6, vol. 1. *Sixth Microgravity Fluid Physics and Transport Phenomena Conference*, National Aeronautics and Space Administration: Cleveland, OH, 620–646 Available from http://gltrs.grc.nasa.gov.
4. Sridhar, K.R., Finn, J.E., and Kliss, M.H. (2000) In-situ resource utilization technologies for mars life support systems. *Adv. Space Res*, 25 (2): 249–255.
5. Ruthven, D.M. (1984) *Principles of Adsorption and Adsorption Processes*; Wiley: New York.
6. Yang, R.T. (1987) *Gas Separation by Adsorption Processes*; Butterworth Publishers: Stoneham, MA.
7. Chihara, K. and Suzuki, M. (1983) Simulation of nonisothermal pressure swing adsorption. *J. Chem. Eng. Japan*, 16: 53–61.
8. Cen, P. and Yang, R.T. (1986) Bulk gas separation by pressure swing adsorption. *Ind. Eng. Chem. Fund.*, 25: 758–767.
9. Kapoor, A. and Yang, R.T. (1989) Kinetic separation of methane-carbon dioxide mixture by adsorption on molecular sieve carbon. *Chem. Eng. Sci.*, 44 (8): 1723–1733.
10. Shin, H. (1995) Separation of a binary gas mixture by pressure swing adsorption: Comparison of different PSA cycles. *Adsorption*, 1: 321–333.
11. Suzuki, T., Sakoda, A., Suzuki, M., and Izumi, J. (1997) Recovery of carbon dioxide from stack gas by piston-driven ultra-rapid PSA. *J. Chem. Eng. Japan*, 30 (6): 1026–1033.
12. Takamura, Y., Narita, S., Aoki, J., Hironaka, S., and Uchida, S. (2001) Evaluation of dual-bed pressure swing adsorption for CO_2 recovery from boiler exhaust gas. *Sep. Purif. Tech.*, 24: 519–528.

13. Rege, S.U., Yang, R.T., Qian, K.Y., and Buzanowski, M.A. (2001) Air-prepurification by pressure swing adsorption using single/layered beds. *Chem. Eng. Sci.*, 56 (8): 2745–2759.
14. Gomes, V.G. and Yee, K.W.K. (2002) Pressure swing adsorption for carbon dioxide sequestration from exhaust gases. *Sep. Purif. Tech.*, 28: 161–171.
15. Park, J.-H., Beum, H.-T., Kim, J.-N., and Cho, S.-H. (2002) Numerical analysis on the power consumption of the PSA process for recovering CO_2 from flue gas. *Ind. Eng. Chem. Res.*, 41 (16): 4122–4131.
16. Yoshida, M., Ritter, J.A., Kodama, A., Goto, M., and Hirose, T. (2003) Enriching reflux and parallel equilization PSA process for concentrating trace components in air. *Ind. Eng. Chem. Res.*, 42 (8): 1795–1803.
17. Taqvi, S.M., Appel, W.S., and LeVan, M.D. (1999) Coadsorption of organic compounds and water vapor on BPL activated carbon. 4. Methanol, ethanol, propanol, butanol, and modeling. *Ind. Eng. Chem. Res.*, 38 (1): 240–250.
18. Farooq, S., Hassan, M.M., and Ruthven, D.M. (1988) Heat effects in pressure swing adsorption systems. *Chem. Eng. Sci.*, 43: 1017–1031.
19. Mahle, J.J., Friday, D.K., and LeVan, M.D. (1996) Pressure swing adsorption for air purification. 1. Temperature cycling and role of weakly adsorbed carrier gas. *Ind. Eng. Chem. Res.*, 35: 2342–2354.
20. Walton, K.S. and LeVan, M.D. (2003) Consistency of energy and material balances for bidisperse particles in fixed-bed adsorption and related applications. *Ind. Eng. Chem. Res.*, 42: 6938–6948.
21. Walton, K.S. and LeVan, M.D. (2005) Adsorbed-phase heat capacities: Thermodynamically consistent values determined from temperature-dependent equilibrium models. *Ind. Eng. Chem. Res.*, 44: 178–182.
22. Nakao, S. and Suzuki, M. (1983) Mass transfer coefficient in cyclic adsorption and desorption. *J. Chem. Eng. Japan*, 16: 114–119.
23. Sladek, K.J., Gilliland, E.R., and Baddour, R.F. (1974) Diffusion on surfaces. II. Correlation of diffusivities of physically and chemically adsorbed species. *Ind. Eng. Chem. Fund.*, 13 (2): 100–105.